The Astrophysical Journal Letters, 903:L24 (6pp), 2020 November 10 https://doi.org/10.3847/2041-8213/abc254

A Unified Accreting Magnetar Model for Long-duration Gamma-Ray Bursts and Some Stripped-envelope Supernovae

W. L. Lin[1], X. F. Wang[1,2,3], L. J. Wang[4], and Z. G. Dai[5,6]
[1] Physics Department and Tsinghua Center for Astrophysics (THCA), Tsinghua University, Beijing 100084, People's Republic of China; linwl@mail.tsinghua.edu.cn, wang_xf@mail.tsinghua.edu.cn
[2] Beijing Planetarium, Beijing Academy of Science and Technology, Beijing 100044, People's Republic of China
[3] Purple Mountain Observatory, Chinese Academy of Science, Nanjing 210008, People's Republic of China
[4] Astroparticle Physics, Institute of High Energy Physics, Chinese Academy of Sciences, Beijing 100049, People's Republic of China
[5] School of Astronomy and Space Science, Nanjing University, Nanjing 210023, People's Republic of China
[6] Key Laboratory of Modern Astronomy and Astrophysics (Nanjing University), Ministry of Education, Nanjing, People's Republic of China
Received 2020 August 23; revised 2020 October 8; accepted 2020 October 18; published 2020 November 4

Abstract

Both the long-duration gamma-ray bursts (LGRBs) and the Type I superluminous supernovae (SLSNe I) have been proposed to be primarily powered by central magnetars. A correlation, proposed between the initial spin period (P_0) and the surface magnetic field (B) of the magnetars powering the X-ray plateaus in LGRB afterglows, indicates a possibility that the magnetars have reached an equilibrium spin period due to the fallback accretion. The corresponding accretion rates are inferred as $\dot{M} \approx 10^{-4}$–$10^{-1}\,M_{\odot}\,\mathrm{s}^{-1}$, and this result holds for the cases of both isotropic and collimated magnetar wind. For the SLSNe I and a fraction of engine-powered normal Type Ic supernovae (SNe Ic) and the broad-lined subclass (SNe Ic-BL), the magnetars could also reach an accretion-induced spin equilibrium, but the corresponding B–P_0 distribution suggests a different accretion rate range, i.e., $\dot{M} \approx 10^{-7}$–$10^{-3}\,M_{\odot}\,\mathrm{s}^{-1}$. Considering the effect of fallback accretion, magnetars with relatively weak fields are responsible for the SLSNe I, while those with stronger magnetic fields could power SNe Ic/Ic-BL. Some SLSNe I in our sample could arise from compact progenitor stars, while others that require longer-term accretion may originate from the progenitor stars with more extended envelopes or circumstellar medium.

Unified Astronomy Thesaurus concepts: Magnetars (992); Supernovae (1668); Gamma-ray bursts (629)

1. Introduction

Rapidly rotating magnetars are promising central engine candidates for some transient astrophysical phenomena. They compete with black holes (BHs) to be the central engines of the gamma-ray bursts (GRBs; e.g., Usov 1992; Dai & Lu 1998; Zhang & Mészáros 2001). They also have been proposed to power the X-ray flares and plateaus (shallow decays) in some GRB afterglows (e.g., Dai et al. 2006; Zhang et al. 2006; Rowlinson et al. 2010, 2013; Dall'Osso et al. 2011; Lü & Zhang 2014; Li et al. 2018; Lin et al. 2018; Stratta et al. 2018). In addition, the magnetar-powered model is invoked to interpret the luminosity evolution of different subclasses of supernovae (SNe; e.g., Kasen & Bildsten 2010; Woosley 2010), such as the normal Type Ic SNe (SNe Ic; e.g., Taddia et al. 2018, 2019), broad-lined SNe Ic (SNe Ic-BL; e.g., Wang et al. 2017a, 2017b), and Type I superluminous supernovae (SLSNe I; e.g., Inserra et al. 2013; Liu et al. 2017; Nicholl et al. 2017; Yu et al. 2017; Blanchard et al. 2018, 2019; Villar et al. 2018; Lin et al. 2020).

In those models, magnetars are usually treated as isolated neutron stars (NSs) that spin down due to the magnetic dipole radiation. In the context of core-collapse explosion, however, the stellar debris could circulate into a disk and interact with a nascent magnetar, which has a strong influence on the spin evolution and outflows of the magnetar (magnetic propeller; e.g., Piro & Ott 2011; Metzger et al. 2018). For a given accretion rate, the magnetar could reach an equilibrium spin period, i.e., $P_{\rm eq} \propto B^{6/7}$ (see also Appendix A), where B is the surface magnetic field of the magnetar. Such a model has been invoked and further developed to study the diverse X-ray light curves of long- and short-duration GRB (LGRB and SGRB) afterglows (Dai & Liu 2012; Gompertz et al. 2014; Gibson et al. 2017, 2018), since the magnetar–disk system could be formed in the cases of both core-collapse explosion and binary compact star mergers. Assuming that the magnetar wind is collimated, Stratta et al. (2018) find a correlation between the surface magnetic field (B) and the initial spin period (P_0) of isolated magnetar engines for X-ray plateaus in GRB afterglows, in agreement with the $B \propto P_{\rm eq}^{7/6}$ relation for the accreting magnetars.

Based on the magnetic propeller model, we tentatively explore the properties of a portion of LGRBs and SNe that can be explained by considering a magnetar as a dominant power source. Our Letter is organized as follows. In Section 2, we collect a sample of transients that are potentially powered by magnetars, including LGRBs with X-ray plateaus, SLSNe I, SNe Ic, and SNe Ic-BL. In Section 3, we show the B–P_0 distribution inferred from isolated magnetars as the central engines for different types of transients, and further discuss its physical implications. A summary is given in Section 4.

2. Data and Sample Selection

Li et al. (2018) systematically studied GRB X-ray plateaus, which are selected from the Neil Gehrels Swift/X-ray Telescope (XRT) data observed during 2004 December–2017 May, and concluded that 19 LGRB X-ray plateaus could be explained by the energy injection from isotropic magnetar wind. Assuming that the magnetar wind is collimated in the plateau phase, however, Lü & Zhang (2014) found more potentially magnetar-powered events from the XRT data obtained between 2005 January and 2013 August. Note that four X-ray plateaus in LGRB afterglows (GRB 060526, GRB

Table 1
The Samples, Models, and References

Transients	Number	Power Source	References
LGRB X-ray plateaus	19	Magnetar (isotropic wind)	Li et al. (2018)
LGRB X-ray plateaus	36	Magnetar (collimated wind)	Lü & Zhang (2014)
SLSNe I	61	Magnetar	Nicholl et al. (2017), Blanchard et al. (2018), Villar et al. (2018), Blanchard et al. (2019), Lin et al. (2020)
SNe Ic-BL without detected LGRBs	11	Magnetar/Magnetar+^{56}Ni	Wang et al. (2017a)
LGRB-SNe	2	Magnetar/Magnetar+^{56}Ni	Greiner et al. (2015), Wang et al. (2017b)
SNe Ic	2	Magnetar+^{56}Ni	Taddia et al. (2018), Taddia et al. (2019)

061110A, GRB 070110, and GRB 120422A) can be explained in both scenarios. We include both of the above two magnetar candidate samples in the following analysis, since the wind configuration is still debated.

The sample of SLSNe I are mainly collected from Nicholl et al. (2017) and Villar et al. (2018), which analyzed multiband light curves of a total of 58 spectroscopically identified SLSNe I based on the magnetar-powered model. In addition, three more SLSNe I (PS16aqv, SN 2017dwh, and SN 2018hti; Blanchard et al. 2018, 2019; Lin et al. 2020) are also included in our sample.

Wang et al. (2017a) invoked the magnetar as an alternative energy source to model the light curves and velocity evolution of 11 SNe Ic-BL without detections of companion LGRBs. For SN 2007ru, SN 2010ah, and PTF10qts, we collect B and P_0 inferred from the pure-magnetar model, while the parameters for the other eight events are determined based on the fits with the magnetar plus ^{56}Ni model, which provides better fits with lower χ^2/dof values.

The magnetar model is also proposed to account for the high luminosity of SN 2011kl (Greiner et al. 2015; Wang et al. 2017c), which is associated with ultralong GRB 111209A. Wang et al. (2017b) fitted the bolometric light curve of SN 1998bw (associated with GRB 980425) with the magnetar plus ^{56}Ni model, and found that the peak and tail of the light curve can be explained by magnetar spin-down. In addition to these two SNe associated with LGRBs (LGRB-SNe), two normal SNe Ic (iPTF15dtg, Taddia et al. 2019; PTF11mnb, Taddia et al. 2018) that are also likely powered by magnetars are included in our sample.

The information of our sample is tabulated in Table 1. From the references listed in Table 1, we collect the parameters (B and P_0) inferred from the models that invoke a magnetar as the dominant energy source.

3. B–P Distribution

3.1. X-Ray Plateaus in LGRB Afterglows

The X-ray plateaus in some LGRB afterglows are observed to persist for $\sim$100–10^5 s before the steeper decline. Assuming that the X-ray plateaus are powered by the isotropic wind from the magnetars, the light curves can be used to constrain the surface magnetic field and initial spin period of magnetars. As seen in Figure 1, magnetars with $P_0 \sim 1$ ms usually possess $B \sim 10^{14}$–10^{15} G, while those with $P_0 \gtrsim 10$ ms are accompanied by a strong magnetic field of $B \sim 10^{15}$–10^{16} G. We perform a linear fit (see Appendix B for the detailed descriptions of the fitting) to the $\log B - \log P_0$ distribution, and find

$$\log B = 14.6^{+0.04}_{-0.05} + (1.13^{+0.11}_{-0.09}) \log P_0, \quad (1)$$

where P_0 is in units of milliseconds. Such a correlation is consistent with the spin equilibrium state for the accreting magnetars ($B \propto P_{\rm eq}^{7/6}$ for a given accretion rate; e.g., Piro & Ott 2011; see also Equation (A3)). It implies that the initial spin period inferred from observations (P_0) could deviate from that of the magnetar at birth, but possibly corresponds to the equilibrium spin period as a result of interaction between the magnetar and surrounding accretion disk. The accretion rates of the disks are inferred as $\dot{M} \approx 10^{-4}$–$0.1\,M_\odot$ s^{-1}. We further estimate the evolutionary timescales for these magnetars to reach the spin equilibrium ($t_{\rm ev} \propto B^{-8/7}\dot{M}^{-3/7}$; Metzger et al. 2018; see also Equation (A4)), which turn out to be $\sim$0.1–1000 s. We consider $t_{\rm ev}$ as the lower limits for the accretion timescales ($t_{\rm acc}$) and show them in Figure 2. Assuming $M_{\rm d} \sim \dot{M} t_{\rm acc}$, the total mass of accretion disk can be constrained to be $M_{\rm d} \gtrsim 10^{-3}$–$0.5\,M_\odot$. We caution that a magnetar could possibly collapse into a BH if it accretes a significant amount of materials and exceeds the maximum mass of a stable NS.[7] Hence, we assume an accretion disk mass of $\lesssim 1\,M_\odot$. Such a disk mass corresponds to an accretion timescale of $\lesssim$10–10^4 s, in agreement with the fallback timescale derived for Wolf–Rayet (WR) stars, i.e., $\sim 10^2$–10^5 s;[8] for a shorter timescale, the fallback materials could come from the core of the progenitors, which suggests an origin of compact progenitor stars for some LGRBs (e.g., Campana et al. 2006; Woosley & Heger 2006).

Notice that only $\sim$20% of X-ray plateaus out of the Li et al. (2018) sample (including LGRB and SGRB X-ray plateaus) are consistent with the energy budget of magnetars, if the magnetar wind is isotropic. They argue that the BHs could be the central engines for most of the X-ray plateaus. If fallback accretion plays a role in the evolution of magnetars, the accreting magnetars could maintain the spin equilibrium on a longer timescale in the presence of an accretion disk, which may provide a natural explanation for the energy that is beyond the millisecond magnetar budget in some cases. Actually, the configuration of magnetar wind is still debated in the context of

[7] Some pulsars with a mass of $\sim 2\,M_\odot$ have been discovered (Demorest et al. 2010; Antoniadis et al. 2013), which sets a lower limit for the maximum mass of NSs ($M_{\rm max}$). Hitherto, there is no consensus on the upper limit of $M_{\rm max}$ (e.g., Lasky et al. 2014; Margalit & Metzger 2017).

[8] The radii ($r_{\rm e}$) of the envelopes of WR stars are $\sim 10^{10}$–10^{12} cm (Koesterke & Hamann 1995). The freefall timescale of the extended envelopes can be estimated by $t_{\rm ff} \sim (r_{\rm e}^3/GM)^{1/2}$, i.e., $100 \lesssim t_{\rm ff} \lesssim 10^5$ s.

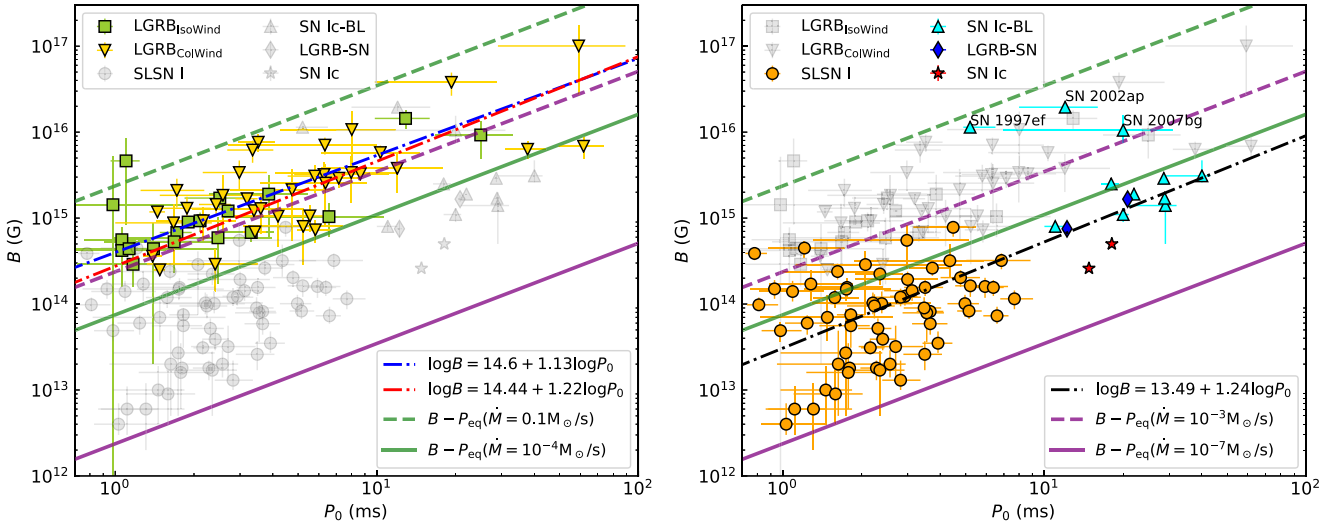

Figure 1. Left panel: B–P_0 distribution for the magnetar engines of LGRB X-ray plateaus (green squares for the isotropic wind model; yellow triangles for the collimated wind model), SLSNe I (gray circles), SNe Ic-BL without LGRBs (gray triangles), LGRB-SNe (gray diamonds), and the normal SNe Ic (gray stars). We show the fitting results for LGRB X-ray plateaus (blue dashed–dotted line for the isotropic wind model, represented by Equation (1); red dashed–dotted line for the collimated wind model, shown by Equation (2)). The expected B–$P_{\rm eq}$ correlations (Equation (A3)) are displayed assuming accretion rates $\dot{M} = 0.1$ (green dashed line), 10^{-3} (purple dashed line), 10^{-4} (green solid line), and 10^{-7} (purple solid line) $M_\odot$ s^{-1}, respectively. Right panel: we highlight the B–P_0 distribution for SLSNe I (orange circles), SNe Ic-BL without LGRBs (cyan triangles), LGRB-SNe (blue diamonds), and the normal SNe Ic (red stars). The black dashed–dotted line represents the best-fit correlation for these SNe (Equation (3)). SN 1997ef, SN 2002ap, and SN 2007bg are labeled due to their significant deviations from the fitting result. LGRB X-ray plateaus are marked in gray. Data references are given in Table 1.

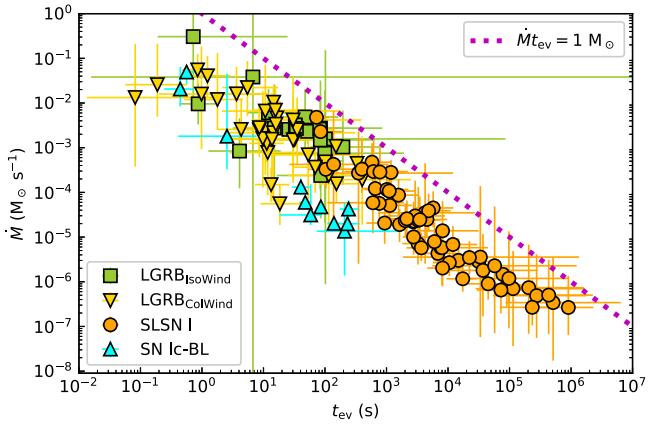

Figure 2. The accretion rate ($\dot{M}$; Equation (A3)) vs. the lower limit of accretion timescale ($t_{\rm ev}$; Equation (A4)) inferred for the magnetar engines of LGRB X-ray plateaus (green squares for the isotropic wind model; yellow triangles for the collimated wind model), SLSNe I (orange circles), and SNe Ic-BL without detected LGRBs (cyan triangles).

LGRB afterglow. Magnetar wind could escape via a collimated jet shortly after the SN explosion (Bucciantini et al. 2009); on a longer timescale, wind could still be channeled into the polar region where the preceding jet drill its way out of the stellar envelope. A large number of X-ray plateaus can be explained by the injection of collimated magnetar wind alongside the GRB jets (Lü & Zhang 2014; Stratta et al. 2018). In Figure 1, we compare the B–P_0 distributions that are derived from different wind models. Although the broader distributions are suggested in the case of collimated wind, they also follow a similar B–P_0 correlation (see also Appendix B), i.e.,

$$\log B = 14.44^{+0.03}_{-0.03} + (1.22^{+0.07}_{-0.06})\log P_0. \quad (2)$$

And the inferred mass inflow rates are similar to those obtained by Stratta et al. (2018) and are also consistent with the results based on the isotropic wind model. Therefore, both results suggest that the central magnetars could experience interactions with the surrounding accretion disks and finally reach a spin equilibrium.

3.2. SLSNe I, SNe Ic, and SNe Ic-BL

Core-collapse SNe usually reach their peak luminosities at tens of days after explosion. Around that time, magnetar wind should be near-isotropic and should contribute most of the rotation energy to heat and/or accelerate the ejecta.

Based on the model fits to the light curves (Nicholl et al. 2017; Blanchard et al. 2018, 2019; Villar et al. 2018; Lin et al. 2020), the magnetar engines of SLSNe I are characterized by a magnetic field of $10^{12} < B \lesssim 10^{14}$ G and a spin with a short period of $1 \lesssim P_0 < 10$ ms (Figure 1). The magnetars with a longer initial spin period appear to have a stronger magnetic field. This correlation possibly suggests that the engine timescale is roughly comparable to the diffusion timescale of ejecta, which corresponds to $B \propto P_0$ (Nicholl et al. 2017). If the physics of accretion-induced spin equilibrium could apply to the cases of SLSNe I, the inferred accretion rates based on Equation (A3) mainly fall between 10^{-7} and 10^{-3} $M_\odot$ s^{-1}.

SNe Ic-BL might be accompanied by the birth of magnetars, since an upper limit of the kinetic energy of SNe Ic-BL (i.e., $\sim$a few 10^{52} erg s^{-1}, model dependent though) is comparable to the maximum rotation energy of a millisecond magnetar (Mazzali et al. 2014). Moreover, some SNe Ic-BL (e.g., SN2010ay and PTF10vqv) are unlikely to be explained by the radioactive ^{56}Ni model and hence the magnetar is invoked as a dominant power source (Wang et al. 2017a). As seen from Figure 1, most SNe Ic-BL without coincident LGRBs in our sample invoke a magnetar with $P_0 \gtrsim 10$ ms and $B \sim 10^{15}$ G, while some events require the magnetic field to be as strong as $\sim 10^{16}$ G. Associated with GRB 980425, SN 1998bw requires $B \approx 1.66 \times 10^{15}$ G for the central magnetar, in agreement with most of its non-GRB peers. Compared with the SLSNe I

magnetars, the magnetar candidates for SNe Ic-BL have a stronger magnetic field and longer initial spin period.

Greiner et al. (2015) reported the observations of a luminous SN Ic SN 2011kl (associated with GRB 111209A), which has intermediate luminosity lying between typical SNe Ic-BL and SLSNe I. Following their fitting results, SN 2011kl could be also powered by a magnetar with an initial spin period of $P_0 \approx 12$ ms and magnetic field of $B \approx 7.5 \times 10^{14}$ G. Two normal SNe Ic (iPTF15dtg and PTF11mnb) require a weaker magnetic field than most SNe Ic-BL and LGRB-SNe in our sample (Taddia et al. 2018, 2019).

We note that, although SLSNe I exhibit distinct spectral features at early times (e.g., Quimby et al. 2011, 2018), their post-peak spectra eventually evolve to resemble those of SNe Ic/Ic-BL (Pastorello et al. 2010; Liu et al. 2017; Blanchard et al. 2019; Nicholl et al. 2019). This suggests an underlying connection among these subtypes of SNe. By fitting the B–P_0 distribution of our SNe samples (including SLSNe I, SNe Ic, and SNe Ic-BL), the following correlation (see also the fitting procedure described in Appendix B) is derived:

$$\log B = 13.49^{+0.1}_{-0.1} + (1.24^{+0.14}_{-0.14}) \log P_0, \quad (3)$$

which is consistent with B–$P_{\rm eq}$ correlation expected for the accreting magnetars at the spin equilibrium state. Although SNe Ic/Ic-BL require different properties of magnetars than SLSNe I, similar accretion rates are inferred for most SNe in our sample.[9] Therefore, the nascent magnetar plus the accretion disk system provide a unified picture to explain the production of SLSNe I, SNe Ic, and SNe Ic-BL. Based on the magnetic propeller model, the central magnetar with a low magnetic field will be accelerated to a millisecond spin period responsible for the energy source powering an SLSN I; conversely, a stronger magnetic field leads to a longer equilibrium spin period of a magnetar, and it hence produces an SN Ic/Ic-BL.

Assuming that magnetars can always reach the spin equilibrium state, the lower limits for accretion timescales in the cases of SLSNe I are estimated as $t_{\rm ev} \sim 10^2$–10^6 s based on Equation (A4), while SNe Ic-BL show a similar $t_{\rm ev}$ distribution to LGRB X-ray plateaus (Figure 2). Although the limits of accretion timescales for most SLSNe I are consistent with the fallback timescale for the envelopes of the compact progenitor stars, a fraction of SLSNe I require longer accretion timescales. Assuming that the accretion timescale ($t_{\rm acc}$) is equivalent to the fallback timescale, the long-term accretion could be due to the fallback of the stellar envelope from large radii or inner ejecta that cannot escape from the central object (Chevalier 1989; Dexter & Kasen 2013). Since early-time bumps observed in some events could be attributed to the cooling of a shocked envelope with a radius of $\gtrsim 500\,R_\odot$ (e.g., Piro 2015; Nicholl & Smartt 2016; Smith et al. 2016), the immediate progenitors of a portion of SLSNe I could be surrounded by largely extended envelopes, in agreement with the first possible scenario allowing for the late accretion. Alternatively, those bumps might suggest the possible existence of circumstellar medium (CSM; Leloudas et al. 2012). In this scenario, reversed shock could be produced by the ejecta–CSM interaction. Then the inner layer of the ejecta would be decelerated by the reverse shock and finally bound to the gravity of the newborn magnetar, contributing to the late accretion. It remains unknown whether SLSNe I could be associated with LGRBs. But it might be a challenge for an LGRB jet to push through the extended envelope or CSM surrounding the progenitor stars of some SLSNe I. For this subclass of SLSNe I, the magnetic field strength is found to be lower than 10^{14} G, which is inconsistent with the magnetic field required by LGRBs.

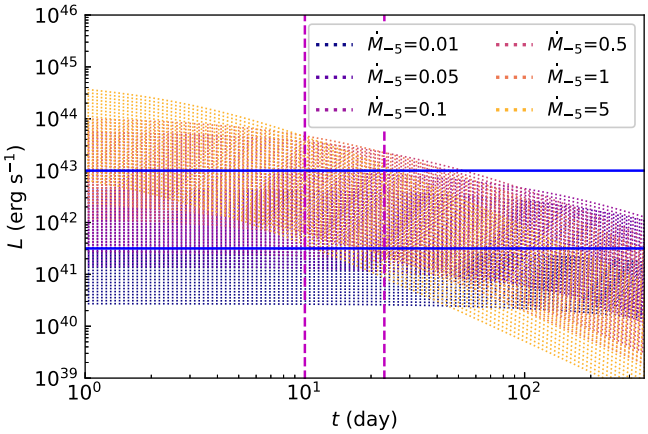

Figure 3. The spin-down luminosity evolution of magnetars with B and P_0, which are adopted (1) from the parameter space limited to $B \in [10^{14}, 10^{16}]$ G and $P_0 \in [10, 100]$ ms, and (2) based on the B–P relation for an accreting magnetar with the accretion rates $\dot{M}_{-5} = \dot{M}/(10^{-5}\,M_\odot\ {\rm s}^{-1}) = 0.01$, 0.05, 0.1, 0.5, 1, 5, respectively. The blue horizon lines show the peak luminosity range of the normal SNe Ic ($41.5 < \log L_{\rm p,Ic} < 43$), and the purple vertical lines mark the major range of the peak time (≈10–23 days; Prentice et al. 2016).

Figure 3 shows some examples of the spin-down luminosity (magnetic dipole radiation luminosity) evolution of isolated magnetars with $B = 10^{14}$–10^{16} G and $P = 10$–100 ms. The spin-down luminosities of those magnetars usually decline below 10^{44} erg s^{-1} after 10 days since explosion, which are insufficient to power SLSNe I according to Arnett's rule (the peak luminosity equals the heating luminosity at peak time). Based on the peak luminosity statistics conducted by Prentice et al. (2016), the majority of normal SNe Ic peak at a luminosity of $\log (L_{\rm p,Ic}) \approx 41.5$–$43$ and at an epoch of 10–23 days after explosion. Since the spin-down luminosities can match the peak luminosities of normal SN Ic during their peak time, it is possible that those magnetars can produce emissions resembling the normal SNe Ic. For an accretion rate between 10^{-7}–$10^{-4}\,M_\odot\,{\rm s}^{-1}$, the accreting magnetars with a magnetic field of $\sim 10^{14}$–10^{15} G could reach an equilibrium spin period of 10–100 ms, and hence possibly power normal SNe Ic. iPTF15dtg exhibits slowly declining light curves and strong Oi λ7774 emission at late phase, which can be explained in the magnetar-powered scenario (Taddia et al. 2019; Nicholl et al. 2019). However, most SNe Ic lack the engine-powered signatures, and ^{56}Ni decay may be the power source. SLSNe I and SNe Ic-BL are preferentially found in dwarf galaxies with low metallicity (e.g., Lunnan et al. 2014; Perley et al. 2016; Schulze et al. 2018; Modjaz et al. 2020). With such low metallicity, stellar wind from massive progenitor stars might be

[9] Note that three SNe Ic-BL (SN 1997ef, SN 2002ap, and SN 2007bg) deviate significantly from the best-fit power-law relation for all of the SNe sample (Equation (3)) in the B–P_0 diagram (Figure 1). They might represent a subset of SNe Ic-BL that are powered by magnetars with the magnetic field being as strong as $\sim 10^{16}$ G. However, we caution that there could be some other reasons for the deviations. Due to the lack of stringent constraints on the magnetar or ^{56}Ni contribution in fitting with the magnetar plus ^{56}Ni model, it is difficult to obtain accurate parameters of the magnetar. In addition, diverse power sources might also lead to a deviation, since both of the magnetar plus ^{56}Ni model and the two-component pure-^{56}Ni model can provide a viable explanation for the emission of SN 1997ef, SN 2002ap, and SN 2007bg (Maeda et al. 2003; Young et al. 2010).

reduced and hence the angular momentum can be sustained to help form a rapidly rotating magnetar. As most SNe Ic prefer higher-metallicity environments (e.g., Modjaz et al. 2020), it is thus expected that only a small subset of SNe Ic are accompanied by the birth of magnetars.

4. Discussions and Conclusions

By involving the fallback accretion effect in the magnetar-powered scenario, we study the correlation between the surface magnetic field (B) and initial spin period (P_0) of magnetar candidates that can account for the emissions of transients, such as LGRB X-ray plateaus, SLSNe I, SNe Ic, and SNe Ic-BL.

In the context of the LGRB with X-ray plateaus, it is still debated whether the magnetar wind is isotropic and collimated in the plateau phase. No matter which wind configuration, however, the initial spin periods and the surface magnetic field of the magnetars are found to follow a positive correlation in agreement with $B \propto P_0^{7/6}$, suggesting that fallback accretion could play a role in the spin evolution of the magnetars. Thus, the initial spin period inferred from observations could correspond to the equilibrium spin period as a result of interaction between the magnetar and surrounding accretion disk. Based on the magnetic propeller model, the accretion rates of the surrounding disks are inferred to be $\dot{M} \approx 10^{-4}$–$10^{-1}\,M_\odot\,\mathrm{s}^{-1}$ and the lower limits for the required accretion timescales are shorter than 1000 s, which are comparable to or shorter than the fallback timescale of the envelope of a WR star. This result is consistent with the proposal of compact progenitor stars as the progenitors of LGRBs, assuming that disk materials fall back from the stellar envelope.

Magnetars are also invoked as an alternative engine to power SNe. On a timescale comparable to the rise time of core-collapse SNe, the magnetar wind should be isotropic. For SLSNe I, SNe Ic, and SNe Ic-BL in our magnetar-powered sample, the B–P_0 distribution is found to be consistent with the physics of accretion-induced spin equilibrium. The inferred accretion rates can be as low as $\dot{M} \approx 10^{-7}$–$10^{-3}\,M_\odot\,\mathrm{s}^{-1}$. Based on the magnetic propeller model, the central magnetars with a low field will be accelerated to a millisecond spin period, and may be able to power SLSNe I; conversely, those with a stronger magnetic field could result in a longer equilibrium spin period, which could explain a portion of SNe Ic/Ic-BL.

For SLSNe I, the accretion timescales are required to be $t_{\rm acc} \gtrsim 10^2$–10^6 s. Assuming that accretion timescale is approximately equal to the fallback time, some SLSNe I of our sample could be produced in the explosions of typical WR stars, while the others that require longer-term accretion could originate from the progenitor stars surrounded by more extended envelopes or CSM, which reconciles with the implication of the early bumps observed in some events (e.g., Leloudas et al. 2012; Piro 2015; Nicholl & Smartt 2016; Smith et al. 2016).

Above discussions are based on a simple method, with which we estimate the constant accretion rates from the B–P_0 distribution inferred from the magnetar-powered models. However, besides the early-time accretion with a constant rate, the late-time decline of the accretion rate can also influence the spin period of the magnetar and hence magnetar outflow can deviate from the magnetic dipole radiation luminosity evolution (e.g., Piro & Ott 2011; Metzger et al. 2018). We expect that more observations and detailed modeling work in the future will provide further clues for the nature of these GRBs and stripped-envelope SNe.

We thank the anonymous referee for constructive comments that helped improve the manuscript. This work is supported by the National Natural Science Foundation of China (NSFC grants 12033003, 11633002, 11761141001, and 11833003) and the National Program on Key Research and Development Project (grants 2016YFA0400803 and 2017YFA0402600). L.J.W. acknowledges support from the National Program on Key Research and Development Project of China (grant 2016YFA0400801).

Appendix A
Magnetic Propeller Model

The interaction between a magnetar with its surrounding disk has an effect on its spin evolution and hence the outflows (e.g., Piro & Ott 2011; Gompertz et al. 2014; Gibson et al. 2017, 2018; Metzger et al. 2018). The interaction can be modeled depending on the relative locations of Alfvén radius ($r_{\rm m}$), corotation radius ($r_{\rm c}$), and light cylinder radius ($r_{\rm L}$). Alfvén radius is usually considered as the inner radius of the disk, where the ram pressure of the inflowing materials balances with the magnetic pressure of the magnetar. It can be given by

$$r_{\rm m} = (GM)^{-1/7} R^{12/7} B^{4/7} \dot{M}^{-2/7}, \tag{A1}$$

where G is the gravitational constant, $M/R/B$ denotes the mass/radius/magnetic field strength of the central magnetar, and $\dot{M}$ is the mass inflow rate at the inner edge of the disk. Given that inflowing materials rotate at the local Keplerian angular velocity, i.e., $\Omega_{\rm K} = (GM/r^3)^{1/2}$, their corotation with the magnetar occurs at a radius of

$$r_{\rm c} = (GM/\Omega^2)^{1/3}, \tag{A2}$$

where $\Omega = 2\pi/P$ and P are the angular velocity and spin period of the magnetar, respectively. The radius of the light cylinder is defined as $r_{\rm L} = c/\Omega$, inside which the magnetic field lines are usually considered to rotate rigidly with the magnetar.

If $r_{\rm m} < r_{\rm c} < r_{\rm L}$, materials at the inner edge of the disk revolve faster than the local magnetic field lines and tend to be funneled before fall onto the surface of the magnetar. Thus, the magnetar gains its angular momentum and subsequently the corotation radius decreases until $r_{\rm c} \sim r_{\rm m}$. Conversely, if $r_{\rm c} < r_{\rm m} \ll r_{\rm L}$, the slow-rotating inner disk is sped up to a super-Keplerian velocity by the magnetar, which results in a mass ejection from disk and sharp spin-down of the magnetar (propeller regime). The spin-down of the magnetar, in return, leads to an increase of $r_{\rm c}$. Consequently, such a magnetar–disk system tends to evolve toward $r_{\rm c} = r_{\rm m}$ if the spin evolution of the magnetar is dominated by the interaction with the accretion disk. When $r_{\rm c}$ equals $r_{\rm m}$, the accreting magnetar would reach an equilibrium spin period (e.g., Piro & Ott 2011)

$$P_{\rm eq} = 2\pi (GM)^{-5/7} R^{18/7} B^{6/7} \dot{M}^{-3/7}. \tag{A3}$$

The equilibrium spin period is independent of the initial spin period of magnetar but correlates with the magnetic field strength and mass inflow rate. With $M = 1.4\,M_\odot$ and $R = 12$

km, therefore, the accretion rate can be estimated from the B–P distribution for accreting magnetars.

Assuming a constant accretion rate, the evolutionary timescale, before a magnetar reaches such a spin equilibrium, can be estimated by (Metzger et al. 2018)

$$t_{\rm ev} \approx \frac{2\pi I/P_{\rm eq}}{\dot{M}(GMr_{\rm m})^{1/2}} = (GM)^{2/7} I R^{-8/7} B^{-8/7} \dot{M}^{-3/7}, \quad \text{(A4)}$$

where $I = 0.35MR^2$ is the moment of inertia. The larger accretion rate and stronger magnetic field correspond to a shorter timescale $t_{\rm ev}$. For an accreting magnetar that spins with an equilibrium period, an estimate of $t_{\rm ev}$ can be considered as the lower limit for the accretion timescale ($t_{\rm acc}$).

Appendix B
Likelihood Function for a Linear Fit

For fitting a linear function ($y = mx + c$) to data with errors on both variables, the likelihood function can be given by (D'Agostini 2005)

$$f \propto \prod_i \frac{1}{\sqrt{\sigma_{y_i}^2 + m^2\sigma_{x_i}^2}} \exp\left[-\frac{(y_i - mx_i - c)^2}{2(\sigma_{y_i}^2 + m^2\sigma_{x_i}^2)}\right], \quad \text{(B1)}$$

where x_i and y_i are the observational quantities, and σ_{x_i} and σ_{y_i} are the corresponding errors.

If there is extra variability of data, which can be parameterized as σ_v, the likelihood function is modified as (D'Agostini 2005)

$$f \propto \prod_i \frac{1}{\sqrt{\sigma_v^2 + \sigma_{y_i}^2 + m^2\sigma_{x_i}^2}} \exp\left[-\frac{(y_i - mx_i - c)^2}{2(\sigma_v^2 + \sigma_{y_i}^2 + m^2\sigma_{x_i}^2)}\right]. \quad \text{(B2)}$$

We fit the data of LGRB X-ray plateaus with Equation (B1) as the likelihood function, and obtain Equation (1) for the isotropic wind model and Equation (1) for the collimated wind model. However, the effect of the extra variability of data (σ_v) should be considered for our SN sample, given the difference in the models (see references listed in Table 1 for details) and the lack of stringent constraint on the magnetar or ^{56}Ni contribution. In fitting, the mean uncertainties of data are adopted as errors for the likelihood function. For the two SNe Ic, the uncertainties of B and P_0 are not given in the literature, so we set the half of the values as the corresponding uncertainties. The fitting result of the SNe is given in Equation (3) with $\sigma_v = 0.52^{+0.05}_{-0.04}$.

ORCID iDs

L. J. Wang https://orcid.org/0000-0002-8352-1359
Z. G. Dai https://orcid.org/0000-0002-7835-8585

References

Antoniadis, J., Freire, P. C. C., Wex, N., et al. 2013, Sci, 340, 448
Blanchard, P. K., Nicholl, M., Berger, E., et al. 2018, ApJ, 865, 9
Blanchard, P. K., Nicholl, M., Berger, E., et al. 2019, ApJ, 872, 90
Bucciantini, N., Quataert, E., Metzger, B. D., et al. 2009, MNRAS, 396, 2038
Campana, S., Mangano, V., Blustin, A. J., et al. 2006, Natur, 442, 1008
Chevalier, R. A. 1989, ApJ, 346, 847
Dai, Z. G., & Liu, R.-Y. 2012, ApJ, 759, 58
Dai, Z. G., & Lu, T. 1998, A&A, 333, L87
Dai, Z. G., Wang, X. Y., Wu, X. F., et al. 2006, Sci, 311, 1127
Dall'Osso, S., Stratta, G., Guetta, D., et al. 2011, A&A, 526, A121
D'Agostini, G. 2005, arXiv:physics/0511182
Demorest, P. B., Pennucci, T., Ransom, S. M., et al. 2010, Natur, 467, 1081
Dexter, J., & Kasen, D. 2013, ApJ, 772, 30
Gibson, S. L., Wynn, G. A., Gompertz, B. P., et al. 2017, MNRAS, 470, 4925
Gibson, S. L., Wynn, G. A., Gompertz, B. P., et al. 2018, MNRAS, 478, 4323
Gompertz, B. P., O'Brien, P. T., & Wynn, G. A. 2014, MNRAS, 438, 240
Greiner, J., Mazzali, P. A., Kann, D. A., et al. 2015, Natur, 523, 189
Inserra, C., Smartt, S. J., Jerkstrand, A., et al. 2013, ApJ, 770, 128
Kasen, D., & Bildsten, L. 2010, ApJ, 717, 245
Koesterke, L., & Hamann, W.-R. 1995, A&A, 299, 503
Lasky, P. D., Haskell, B., Ravi, V., et al. 2014, PhRvD, 89, 047302
Leloudas, G., Chatzopoulos, E., Dilday, B., et al. 2012, A&A, 541, A129
Li, L., Wu, X.-F., Lei, W.-H., et al. 2018, ApJS, 236, 26
Lin, W.-L., Wang, L.-J., & Dai, Z.-G. 2018, ApJ, 855, 67
Lin, W. L., Wang, X. F., Li, W. X., et al. 2020, MNRAS, 497, 318
Liu, L.-D., Wang, S.-Q., Wang, L.-J., et al. 2017, ApJ, 842, 26
Liu, Y.-Q., Modjaz, M., & Bianco, F. B. 2017, ApJ, 845, 85
Lü, H.-J., & Zhang, B. 2014, ApJ, 785, 74
Lunnan, R., Chornock, R., Berger, E., et al. 2014, ApJ, 787, 138
Maeda, K., Mazzali, P. A., Deng, J., et al. 2003, ApJ, 593, 931
Margalit, B., & Metzger, B. D. 2017, ApJL, 850, L19
Mazzali, P. A., McFadyen, A. I., Woosley, S. E., et al. 2014, MNRAS, 443, 67
Metzger, B. D., Beniamini, P., & Giannios, D. 2018, ApJ, 857, 95
Modjaz, M., Bianco, F. B., Siwek, M., et al. 2020, ApJ, 892, 153
Nicholl, M., Berger, E., Blanchard, P. K., et al. 2019, ApJ, 871, 102
Nicholl, M., Guillochon, J., & Berger, E. 2017, ApJ, 850, 55
Nicholl, M., & Smartt, S. J. 2016, MNRAS, 457, L79
Pastorello, A., Smartt, S. J., Botticella, M. T., et al. 2010, ApJL, 724, L16
Perley, D. A., Quimby, R. M., Yan, L., et al. 2016, ApJ, 830, 13
Piro, A. L. 2015, ApJL, 808, L51
Piro, A. L., & Ott, C. D. 2011, ApJ, 736, 108
Prentice, S. J., Mazzali, P. A., Pian, E., et al. 2016, MNRAS, 458, 2973
Quimby, R. M., De Cia, A., Gal-Yam, A., et al. 2018, ApJ, 855, 2
Quimby, R. M., Kulkarni, S. R., Kasliwal, M. M., et al. 2011, Natur, 474, 487
Rowlinson, A., O'Brien, P. T., Metzger, B. D., et al. 2013, MNRAS, 430, 1061
Rowlinson, A., O'Brien, P. T., Tanvir, N. R., et al. 2010, MNRAS, 409, 531
Schulze, S., Krühler, T., Leloudas, G., et al. 2018, MNRAS, 473, 1258
Smith, M., Sullivan, M., D'Andrea, C. B., et al. 2016, ApJL, 818, L8
Stratta, G., Dainotti, M. G., Dall'Osso, S., et al. 2018, ApJ, 869, 155
Taddia, F., Sollerman, J., Fremling, C., et al. 2018, A&A, 609, A106
Taddia, F., Sollerman, J., Fremling, C., et al. 2019, A&A, 621, A64
Usov, V. V. 1992, Natur, 357, 472
Villar, V. A., Nicholl, M., & Berger, E. 2018, ApJ, 869, 166
Wang, L. J., Cano, Z., Wang, S. Q., et al. 2017a, ApJ, 851, 54
Wang, L. J., Yu, H., Liu, L. D., et al. 2017b, ApJ, 837, 128
Wang, S.-Q., Cano, Z., Wang, L.-J., et al. 2017c, ApJ, 850, 148
Woosley, S. E. 2010, ApJL, 719, L204
Woosley, S. E., & Heger, A. 2006, ApJ, 637, 914
Young, D. R., Smartt, S. J., Valenti, S., et al. 2010, A&A, 512, A70
Yu, Y.-W., Zhu, J.-P., Li, S.-Z., et al. 2017, ApJ, 840, 12
Zhang, B., Fan, Y. Z., Dyks, J., et al. 2006, ApJ, 642, 354
Zhang, B., & Mészáros, P. 2001, ApJL, 552, L35